injection of the anti-γ-enolase autoantibodies resulted in retinal damage in rats [9]. On the other hand, Schwartz and her colleagues reported that T cell-mediated autoimmunity plays a crucial role in the progression of glaucomatous optic neuropathy in mice and rats, and suggested possibility of immunotherapy for neuroprotection against glaucomatous optic neuropathy [10,11]. Taken together, immunological investigation of the glaucomatous optic neuropathy may lead to the development of a novel concept for the treatment of glaucoma in addition to the presently used IOP-lowering treatments.

Herein, we present evidence that neurofilament protein may be a novel autoantigen that is involved in autoimmunity and leads to the development of glaucomatous optic neuropathy. Also, our immunological analysis revealed that there was a statistical association between the HLA class II allele and the presence of autoantibodies directed against neurofilament protein in patients which suggests that there is HLA-linked genetic control of autoimmune glaucoma.

2. Materials and methods

2.1. Patients

In this study, 65 patients with glaucoma were subjected to analysis. The mean age (±S.D.) in the patients was 61.3 ± 12.6 years old (range, 22–78 years old). The patients included 34 males and 31 females. In 30 of the 65 patients, the glaucoma was diagnosed as normal tension glaucoma (NTG) based upon (1) open iridocorneal angles without any peripheral anterior synechia, (2) no evidence of elevation in intraocular pressure (>21 mmHg), (3) the presence of glaucomatous (or glaucoma-like) changes in visual fields and optic nerve appearance and (4) exclusion of any other causes of optic neuropathy. The remaining 35 patients were diagnosed as having primary open angle glaucoma with glaucomatous optic neuropathy and had a history of high intraocular pressure (>21 mmHg). Additionally, in this study, 42 patients with Vogt–Koyanagi–Harada disease (VKH), 31 patients with Behçet's disease (BD) with ocular complications, 30 patients with the opticospinal form of multiple sclerosis (OS-MS) and 30 patients with the conventional form of multiple sclerosis (C-MS) were subjected to immunological analysis. Sixty-nine normal healthy volunteers were used as healthy controls in the present study. Peripheral venous blood samples were immediately subjected to serum separation and stored at −80 °C before use. All subjects were unrelated Japanese living in Japan and informed consents were obtained from all subjects prior to blood sampling. This study was done according to the tenets of the Declaration of Helsinki.

2.2. Immunoscreening

A rat retinal cDNA expression library was purchased from Strategene (La Jolla, CA, USA). The immunoscreening method used was a modification of our published methods [12,13]. Sera were diluted in Tris-buffered-saline (TBS). Recombinant phages at a concentration of 1×10^4/15 cm plate were amplified for 6 h at 42 °C, then transferred onto nitrocellulose filters Hybond-c extra (Amersham, Buckinghamshire, England), pretreated with isopropyl b-D-thiogalactoside (Wako, Osaka, Japan), and incubated for an additional 3 h at 37 °C to transfer the encoded proteins onto the filter membranes. Membranes were then removed from plate and blocked with 5% (w/v) skim milk/TBS. After washing with TBS containing 0.05% Tween 20 (TBS-T), membranes were incubated in 2 h at 27 °C. This was followed by incubation in horseradish peroxidase (HRP)-conjugated mouse anti-human IgG (Southern Biotechnology Associates Inc., Birmingham, AL) for 1 h at room temperature. The membranes were washed in TBS-T and TBS and incubated with ECL RPN 2106 (Amersham) for 1 min, and exposed to autoradiographic film to detect any antibody-reactive phage plaques. Positive recombinant clones were subcloned and retested for sera reactivity as described above. A total of 1.5×10^6 recombinant clones were screened, using sera from three glaucomatous patients.

2.3. Sequence analysis of identified cDNA clones

Immunoreactive phage clones were subjected to in vivo excision of pBluescript phagemid, using the ExAssist helper phage/SOLR strain system (Stratagene). Plasmid DNA was purified, using QIAGEN Plasmid Midi Kits (Tokyo, Japan) cDNA inserts were sequenced, using an ABI Prism (Perkin-Elmer, Norwalk, CT) automated DNA sequencer and for sequence alignments we used BLAST software on NCBI and Genone Net.

2.4. Enzyme-linked immunosorbent assay

Detection and tituration of antibodies reactive to purified bovine neurofilament protein (PROGEN, Heidelberg, Germany) were done, using a direct enzyme-linked immunosorbent assay (ELISA). Microtiter plates (96-well) (NUNC, Denmark) were coated with neurofilamemt protein in PBS (pH 7.4) for 10 h at 4 °C. The plates were then washed with PBS containing 0.05% Tween 20 (PBS-T) and blocked with 5% skim milk/PBS for 2 h at room temperature. The plates were washed with PBS-T and incubated for 2 h at room temperature with serum samples diluted at 1:100 with 1% skim milk/PBS. The plates were washed in PBS-T and 100 μl of HRP-conjugated mouse anti-human IgG diluted at 1:2000 with 1% skim milk/PBS was added to each well and then followed by incubation at room temperature for 1 h. The plates were washed with PBS-T, and 100 μl solution of *o*-phenylenediamine (Sigma Fast: Sigma Chemical Co., St. Louis, MO) was added to each well. After 15 min, the reaction was stopped by adding 100 μl of 4 M H_2SO_4, and the optical density (OD) at 490 nm was determined, using a Model 550 microplate reader (Bio-Rad, Hercules, CA). The reactiv-

ities of autoantibodies are expressed as the relative value of the OD unit in which the OD value for the serum sample of patient TT was estimated to be 100 OD units.

2.5. HLA-DRB1 typing

Extraction of genomic DNAs was performed by sodium dodecyl sulphate and proteinase C treated peripheral blood cells from 55 patients with glaucoma and 57 healthy controls. HLA-DRB1 genes were amplified by polymerase chain reaction (PCR) method and typed by the PCR-restriction fragment length polymorphism (RFLP) method as described elsewhere [14].

3. Results

3.1. Identification of immunoreactive cDNA clones

With a serum sample obtained from a patient with NTG (a 58-year-old man), 4.0×10^5 phage plaques in the rat retinal cDNA library were immunoscreened. Seven positive immunoreactive clones were identified. Their partial sequences of inserted DNAs and subsequent computer analysis revealed that they were derived from two different sequences. The deduced amino acid sequences of six clones were identical to rat neurofilament protein and another clone encoded for the Wiskott-Aldrich syndrome proteins family verprolin homologous protein3 (WAVE3). Thus, our immunoscreening studies revealed the presence of anti-rat neurofilament protein IgG antibodies in a patient with NTG.

3.2. Comparison of the prevalence of anti-bovine neurofilament IgG in sera from patients with glaucoma, other diseases and healthy controls

To determine if the autoimmunity directed against the neurofilament protein is associated with glaucomatous optic nerve damage, serum samples obtained from 65 glaucomatous patients, 42 patients with VKH, 31 patients with BD, 60 patients with MS and 69 healthy controls were tested for their reactivity to neurofilament protein. Because purified human neurofilament protein was not available for the present studies, bovine neurofilament protein (68-kD light subunit) was purchased from PROGEN (Heidelberg, Germany) and was used for the following experiments to determine the levels of antibody titers in ELISA in sera from the various patients and normal volunteers. Computer analysis of the deduced amino acid sequences demonstrated by the homology of the 68-kD light subunit of neurofilament (NF-L) between bovine and human, human and rat, rat and bovine was 78–81%.

Fig. 1 shows scatter grams of individual serum titers of the anti-NF-L IgG. The results were expressed as the relative value of OD unit. To determine the cut-off level for positivity of anti-NF-L in the 69 healthy controls, titer levels were measured. The mean (±S.D.) titer level of the anti-NF-L IgG was 7.5 ± 8.7. Thus, we regarded the mean value plus two times the standard deviation, $7.5 + 8.7 \times 2 = 24.9$, as the cut-off level for this ELISA analysis. The prevalence of anti-NF-L IgG in patients and healthy controls is shown in Table 1. Our ELISA experiments showed that the measured titer levels of anti-NF-L IgG were higher than the cut-off level, found in 12 (18.5%) of the 65 glaucomatous patients and in four (5.8%) of the 69 normal controls ($P = 0.022$, Fisher's exact test). The difference in the percentage of autoantibody-positive subjects was statistically significant between these two groups.

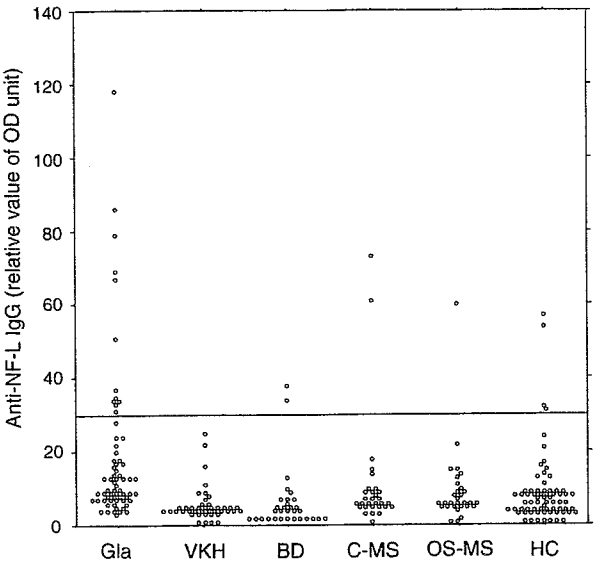

Fig. 1. Distribution of the titer of anti-bovine NF-L IgG antibodies in patients with glaucoma (Gla), Vogt–Koyanagi–Harada disease (VKH), Behçet's disease (BD), opticospinal form of multiple sclerosis (OS-MS), conventional form of multiple sclerosis (C-MS) and healthy controls (HC). Data were expressed as the relative value of optical density (OD) unit in which the OD value for the serum sample of patient TT was estimated to be 100 OD units. To determine the cut-off level for the positivity of anti-NF-L IgG, the levels were measured in 69 healthy controls. The mean (±S.D.) titer level of the anti-NF-L IgG was 7.5 ± 8.7. Thus, we regarded the mean value plus two times the standard deviation (24.9), as the cut-off level for this ELISA analysis (indicated by the line).

Table 1
Prevalence of anti-NF-L IgG evaluated by ELISA in sera from patients with glaucoma, disease controls and healthy controls

Diagnosis	Anti-NF-L IgG positive donors	Frequency (%)
Glaucoma	12/65	18.5*
VKH	0/42	0.0
BD	2/31	6.5
OS-MS	1/30	3.3
C-MS	2/30	6.7
HC	4/69	5.8*

VKH, Vogt–Koyanagi–Harada disease; BD, Behçet's disease; OS-MS, opticospinal form of multiple sclerosis; C-MS, conventional form of multiple sclerosis; HC, healthy control.

* Statistically significant difference in frequency of anti-NF-L IgG autoantibodies between HC and glaucom groups ($P = 0.022$, Fisher's exact test).

Table 2
Allele frequency of HLA-DRB1 in patients with glaucoma and normal controls

Allele	Glaucoma ($n=55$)		Control subject ($n=57$)		P-value
	n	AF	n	AF	
DRB1*0101	8	0.145	9	0.158	NS
DRB1*0301	1	0.018	1	0.018	NS
DRB1*0401	1	0.018	1	0.018	NS
DRB1*0403	2	0.036	2	0.035	NS
DRB1*0405	16	0.291	12	0.211	NS
DRB1*0406	4	0.073	5	0.088	NS
DRB1*0410	2	0.036	2	0.035	NS
DRB1*0802	4	0.073	3	0.053	NS
DRB1*0803	10	0.182	12	0.211	NS
DRB1*0901	17	0.301	15	0.263	NS
DRB1*1101	1	0.018	3	0.053	NS
DRB1*1201	1	0.018	4	0.07	NS
DRB1*1301	1	0.018	1	0.018	NS
DRB1*1302	8	0.145	9	0.158	NS
DRB1*1401	2	0.036	0	0	NS
DRB1*1405	4	0.073	3	0.053	NS
DRB1*1406	3	0.055	0	0	NS
DRB1*1501	8	0.145	8	0.14	NS
DRB1*1502	16	0.291	14	0.246	NS
DRB1*1602	1	0.018	1	0.018	NS

AF: allele frequency; NS: not significant; Chi-square test.

We measured antibody titer levels of anti-NF-L IgG in serum samples obtained from patients with various ocular diseases. ELISA studies showed that the titer levels higher than the cut-off value were found in none (0%) of the 42 patients with VKH, two (6.5%) of the 31 patients with BD, one (3.3%) of the 30 patients with OS-MS and two (6.7%) of the 30 patients with C-MS. As shown in Table 1, there were no statistically significant differences in the prevalence of the titer levels of anti-NF-L IgG that were higher than the cut-off level between the normal controls and each group. The age distribution is not significantly different between anti-NF-L IgG positive and negative donors in each group of patients as well as healthy controls (data not shown).

3.3. HLA-DRB1 allele frequency

There were no statistically significant differences in the allele frequency of HLA-DRB1 between normal controls and the combined glaucomatous patient group (Table 2). We divided the glaucomatous patients into two groups based upon their anti NF-L IgG titer levels. In the anti NF-L IgG positive group, which was composed of patients with anti NF-L IgG titer levels higher than the cut-off level, HLA-DRB1*1502 allele was observed in seven (58.3%) of the 12 patients. On the other hand, in the anti-NF-L IgG negative group, which was composed of patients with anti-NF-L IgG titer levels equal to or below the cut-off level, the allele was only found in seven (16.3%) of the 43 patients. The differences in prevalence of anti NF-L IgG were statistically significant between these two groups ($P<0.05$, Chi-square test) (Table 3).

Table 3
Difference between anti-NF-L IgG positive patients and negative patients in frequency of DRB1 alleles

Allele	Anti-NF-L IgG positive patients ($n=12$)		Anti-NF-L IgG negative patients ($n=43$)		P-Value
	n	Frequency	n	Frequency	
DRB1*0101	1	0.083	5	0.116	NS
DRB1*0301	0	0.000	1	0.023	NS
DRB1*0401	0	0.000	1	0.023	NS
DRB1*0403	0	0.000	2	0.047	NS
DRB1*0405	4	0.333	10	0.233	NS
DRB1*0406	0	0.000	4	0.093	NS
DRB1*0410	0	0.000	2	0.047	NS
DRB1*0802	0	0.000	4	0.093	NS
DRB1*0803	2	0.167	6	0.14	NS
DRB1*0901	2	0.167	11	0.256	NS
DRB1*1101	1	0.083	0	0	NS
DRB1*1201	0	0.000	1	0.023	NS
DRB1*1301	1	0.083	0	0	NS
DRB1*1302	2	0.167	6	0.14	NS
DRB1*1401	0	0.000	2	0.047	NS
DRB1*1405	1	0.083	3	0.07	NS
DRB1*1406	2	0.167	1	0.023	NS
DRB1*1501	1	0.083	7	0.163	NS
DRB1*1502	6	0.500	9	0.21	<0.05
DRB1*1602	0	0.000	1	0.023	NS

NS: not significant; Chi-square test.

4. Discussion

Recent studies have revealed that glaucomatous optic neuropathy may be caused by many risk factors such as ischemia, genetic background, glutamate and immune response in addition to intraocular pressure [1]. Among these, involvement of the immune response in the pathogenesis of glaucomatous optic neuropathy has been the focus of investigations. Several investigators have reported the presence of autoantibodies in glaucomatous patients [5–8,15,16]. Also, recent studies have suggested that T cell-mediated immune response might play a crucial role in the progression of glaucomatous optic nerve damages in animal experimental models [10,11,17,18]. These findings have shed light on new aspects for understanding of the pathogenesis and treatment of glaucomatous optic neuropathy. Based on these findings, we conducted a series of experiments in the present study in an attempt to further elucidate a role for involvement of autoimmunity and the immunogenetic background, in glaucomatous optic nerve damage.

In previous studies, Western blot analysis was used for the identification of autoantibodies in serum samples obtained from glaucomatous patients [5–8,16]. These methods are useful for identification of autoantibodies directed against antigens that have a large amount of expression. However, this method has a potential risk in that it can exclude the detection of important antigens if the autoantigens are barely expressed. For this reason it is possible that autoantigens associated with the progression of glaucomatous optic neuropathy

may escape detection of a Western blot analysis. Thus, in order to better understand the immunological mechanisms of glaucomatous optic neuropathy, more sensitive and reliable technique needs to be applied. In the present study, we applied SEREX method to the identification of glaucoma-associated autoantigens. This molecular biological method enabled us to detect autoantigens regardless of whether the expression was very low, and to easily accomplish subsequent molecular cloning of genes that encode for the autoantigen.

With the aid of the SEREX method in our previous studies, we have been able to identify disease-associated autoantigens in patients with VKH and cancers [12,19–21]. In VKH, T helper 1 type T cells-mediated cellular immunity plays a dominant role in the pathogenesis [22,23]. In cases of glaucoma, some investigators have suggested the involvement of T cell-mediated cellular immunity play a role in the neuroprotection against glaucomatous optic neuropathy whereas T helper 2 type T cells-mediated humoral immunity should be regarded as the main cause for the production of autoantibodies [11,17]. Thus, presently, our understanding on immunological mechanisms associated with glaucomatous optic neuropathy is far from satisfactory. Therefore, we considered the use of SEREX to be suitable for our aims of elucidating the mechanism of autoimmunity in glaucoma.

In the present study, we identified neurofilament proteins as the candidate target autoantigens associated with glaucoma. Neurofilament proteins are known to be major intermediate filaments that are present in the nervous system and construct the axonal cytoskeleton. So far, three types of subunits for neurofilament have been identified; the 68-kD light subunit (NF-L), the 160-kD medium subunit (NF-M) and the 200-kD heavy subunit (NF-H). NF-L constructs the backbone of neurofilament while NF-M and NF-H are localized on the periphery of NF-L. Targeted disruption of the NF-L gene results in reduction of radial growth of neuronal axons [24]. It has been reported that abnormal accumulation of neurofilament is the pathological hallmark of some neurodegenerative diseases such as amyotrophic lateral sclerosis (ALS), Lewy-body-type dementia and Parkinson's disease [25–27]. The presence of autoantibodies directed against NF proteins has been reported in patients with progressive MS [28,29]. From the viewpoint of glaucoma, it has been reported that expression of NF proteins in retinal ganglion cells reduced in glaucomatous patients [30,31].

In our study, use of the SEREX method and a serum sample of a patient with normal tension glaucoma, allowed us to identify neurofilament protein as a candidate autoantigen associated with glaucomatous optic neuropathy. Our results showed a statistically significant difference between the prevalence of anti-NF-L IgG in normal controls and glaucomatous patients, but not between normal controls and other diseases such as VKH, BD and MS. In glaucoma, retinal ganglion cells and their axons specifically deteriorate whereas it is the uveal tissues that are mainly involved in VKH. However, in BD and MS as well as glaucoma, optic nerve damage dose occur. Thus, our positive results that showed the prevalence of a high titer of anti-NF-L IgG in glaucomatous patients might suggest that this immune response may be associated with a certain sub-group of glaucomatous patients. One of the most important points that need to be addressed concerns what mechanisms segregate this sub-group of glaucomatous patients with regards to the immunological reaction against NF-L. This question may be partially answered by our additional results for the typing of HLA class II alleles in glaucomatous patients.

The association between glaucoma and HLA class II allele has been previously reported [32,33]. In the present study, we document the frequency of HLA-DRB1 allele in Japanese glaucomatous patients for the first time. A statistically significant difference was revealed in the allele frequency of HLA-DRB1*1502 between the anti-NF-L IgG positive and negative groups in glaucomatous patients. Our finding suggests that specific HLA class II alleles or genes in with a strong linkage with disequilibrium with HLA-DRB1*1502 may play an important role in the production of autoantibodies in glaucomatous patients. The presence of autoantibodies reactive to retinal and/or optic nerve antigens may result from prolonged exposure of the immune system to autoantigens caused by glaucomatous optic nerve damage. However, we cannot exclude another possibility that the autoantibody-associated immune response may deteriorate (or inhibit) the progression of glaucomatous optic neuropathy. Taken into consideration together, we can hypothesize that the immunogenetic background associated with HLA class II alleles may control susceptibility to autoimmunity. Our hypothesis may shed new light for understanding the presence of autoantibodies in glaucomatous patients. Further studies are necessary to elucidate the relationships between HLA class II alleles and the immunological abnormality in glaucoma.

In conclusion, we have identified neurofilament proteins as a novel autoantigens associated with glaucomatous optic nerve damage. This autoimmunity was found in some but not all glaucomatous patients, and was not found in patients with other ocular diseases. HLA-DRB1*1502 allele was also significantly associated with high titer of anti-NF-L IgG in glaucomatous patients, suggesting the importance of HLA class II-linked genes in the development of autoimmunity in glaucoma.

References

[1] Vorwerk CK, Gorla MS, Dreyer EB. Surv Ophthalmol 1999;43:S142–50.
[2] Osborne NN, Ugarte M, Chao M, Chidlow G, Bae JH, Wood JP, et al. Surv Ophthalmol 1999;43:S102–28.
[3] Kerrigan LA, Zack DJ, Quigley HA, Smith SD, Pease ME. Arch Ophthalmol 1997;115:1031–5.
[4] Quigley HA, Nickells RW, Kerrigan LA, Pease ME, Thibault DJ, Zack DJ. Invest Ophthalmol Vis Sci 1995;36:774–86.
[5] Romano C, Barrett DA, Li Z, Pestronk A, Wax MB. Invest Ophthalmol Vis Sci 1995;36:1968–75.
[6] Tezel G, Seigel GM, Wax MB. Invest Ophthalmol Vis Sci 1998;39:2277–87.

[7] Tezel G, Edward DP, Wax MB. Arch Ophthalmol 1999;117:917–24.
[8] Yang J, Tezel G, Patil RV, Romano C, Wax MB. Invest Ophthalmol Vis Sci 2001;42:1273–6.
[9] Maruyama I, Maeda T, Okisaka S, Mizukawa A, Nakazawa M, Ohguro H. Jpn J Ophthalmol 2002;46:1–12.
[10] Fisher J, Levkovitch-Verbin H, Schori H, Yoles E, Butovsky O, Kaye JF, et al. J Neurosci 2001;21:136–42.
[11] Schori H, Kipnis J, Yoles E, WoldeMussie E, Ruiz G, Wheeler LA, et al. Proc Natl Acad Sci USA 2001;98:3398–403.
[12] Yamada K, Senju S, Nakatsura T, Murata Y, Ishihara M, Nakamura S, et al. Biochem Biophys Res Commun 2001;280:1169–76.
[13] Nakatsura T, Senju S, Ito M, Nishimura Y, Itoh K. Eur J Immunol 2002;32:826–36.
[14] Shindo Y, Inoko H, Yamamoto T, Ohno S. Br J Ophthalmol 1994;78:223–6.
[15] Wax MB, Tezel G, Kawase K, Kitazawa Y. Ophthalmology 2001;108:296–302.
[16] Maruyama I, Ohguro H, Ikeda Y. Invest Ophthalmol Vis Sci 2000;41:1657–65.
[17] Schwartz M. Surv Ophthalmol 2001;45:S256–60 (discussion S273–6).
[18] Bakalash S, Kipnis J, Yoles E, Schwartz M. Invest Ophthalmol Vis Sci 2002;43:2648–53.
[19] Yamada K, Senju S, Shinohara T, Nakatsura T, Murata Y, Ishihara M, et al. Immunol Lett 2001;78:161–8.
[20] Nakatsura T, Senju S, Yamada K, Jotsuka T, Ogawa M, Nishimura Y. Biochem Biophys Res Commun 2001;281:936–44.
[21] Monji M, Senju S, Nakatsura T, Yamada K, Sawatsubashi M, Inokuchi A, et al. Biochem Biophys Res Commun 2002;294:734–41.
[22] Yamaki K, Gocho K, Hayakawa K, Kondo I, Sakuragi S. J Immunol 2000;165:7323–9.
[23] Gocho K, Kondo I, Yamaki K. Invest Ophthalmol Vis Sci 2001;42:2004–9.
[24] Zhu Q, Couillard-Despres S, Julien JP. Exp Neurol 1997;148:299–316.
[25] Julien JP. Curr Opin Neurobiol 1999;9:554–60.
[26] Al-Chalabi A, Andersen PM, Nilsson P, Chioza B, Andersson JL, Russ C, et al. Hum Mol Genet 1999;8:157–64.
[27] Goldman JE, Yen SH, Chiu FC, Peress NS. Science 1983;221:1082–4.
[28] Silber E, Semra YK, Gregson NA, Sharief MK. Neurology 2002;58:1372–81.
[29] Eikelenboom MJ, Petzold A, Lazeron RH, Silber E, Sharief M, Thompson EJ, et al. Neurology 2003;60:219–23.
[30] Naskar R, Wissing M, Thanos S. Invest Ophthalmol Vis Sci 2002;43:2962–8.
[31] Vickers JC, Hof PR, Schumer RA, Wang RF, Podos SM, Morrison JH. Aust NZ J Ophthalmol 1997;25:239–43.
[32] Gil-Carrasco F, Vargas-Alarcon G, Zuniga J, Tinajero-Castaneda O, Hernandez-Martinez B, Hernandez-Pacheco G, et al. Am J Ophthalmol 1999;128:297–300.
[33] Ferreri G, D'Andrea A, Castagna I, Rechichi C, Pettinato G, D'Andrea D. Acta Ophthalmol Scand Suppl 1998:17–9.

JOURNAL OF BIOSCIENCE AND BIOENGINEERING
Vol. 99, No. 1, 30–37. 2005
DOI: 10.1263/jbb.99.030

Reconstitution and Function of *Tetragenococcus halophila* Chaperonin 60 Tetradecamer

AMONLAYA TOSUKHOWONG,[1] JIRO NAKAYAMA,[1] YOSHIMITSU MIZUNOE,[2] SHINYA SUGIMOTO,[1] DAISUKE FUKUDA,[1] AND KENJI SONOMOTO[1]*

Laboratory of Microbial Technology, Division of Microbial Science and Technology, Department of Bioscience and Biotechnology, Faculty of Agriculture, Graduate School, Kyushu University, 6-10-1 Hakozaki, Higashi-ku, Fukuoka 812-8581, Japan[1] and Department of Bacteriology, Faculty of Medical Sciences, Graduate School, Kyushu University, 3-1-1 Maidashi, Higashi-ku, Fukuoka 812-8582, Japan[2]

Received 14 July 2004/Accepted 5 October 2004

Tetragenococcus halophila **originally isolated from soy sauce is a halophilic lactic acid bacterium which can grow under 4 M sodium chloride. *T. halophila* chaperonin composed of a core moiety of chaperonin 60 (cpn60) and a lid moiety of chaperonin 10 (cpn10), is thought to contribute to host halotolerant capability. In this report, we reconstituted and characterized the core complex of *T. halophila* chaperonin by using a recombinant *T. halophila* cpn60 (Tcpn60) overexpressed in *Escherichia coli*. The reconstitution of Tcpn60 was performed in the presence of 10 mM $MgCl_2$, 2 mM ATP and 0.8 M $(NH_4)_2SO_4$ and the resultant oligomer was purified by gel filtration chromatography. Electron microscopy of the reconstituted Tcpn60 revealed a double toroidal tetradecameric structure that is characteristic of bacterial cpn60. The *T. halophila* tetradecamer cpn60 exhibited an ATPase activity and a refolding activity of both chemically and thermally denatured enolases under wide range of salt concentrations. Furthermore, we demonstrated that heterologous expression of Tcpn60 allowed the normal growth of host *Escherichia coli* cells under salt stress conditions and this effect was further enhanced by co-expression with Tcpn10. These results suggested that Tcpn60 contributes to the halotolerance property of *T. halophila* cell as a tetradecamer complex, probably associated with the Tcpn10 complex.**

[**Key words:** chaperonin 60, halophilic, *Tetragenococcus halophila*, GroEL, reconstitution]

The lactic acid bacterium *Tetragenococcus halophila* is a tetrad-forming gram-positive coccus showing moderately halotolerance. *T. halophila* can grow under salt concentrations ranging from 0.5% (0.086 M) to 30% (5.1 M) (10% [1.71 M] is optimum) and is suitable for use in brine fermentations such as the brewing of soy sauce (1). However, little is known about the halotolerance mechanism of moderately halophilic bacteria, particularly lactic acid bacteria. Robert *et al.* (2) have indicated that compatible solutes such as glycine betaine prevent the accumulation of sodium ions to a level inhibiting growth. They also showed that the concentration of potassium ions instead of sodium ions increased under high salinity conditions with compatible solutes. This suggested that the intracellular environment still suffers from high salinity even with protection by compatible solutes. We are interested in the mechanism of how cellular proteins can be protected from denaturing by high salinity in *T. halophila* cells and have studied on the machinery of *T. halophila* molecular chaperones (3–5).

Chaperonins are molecular chaperones and are a family of ubiquitous proteins highly conserved among almost all organisms from prokaryotes to eukaryotes (6). The function of chaperonins is to assist correct folding of nascent proteins or refolding of denatured proteins (7, 8). In addition to this function, chaperonins contribute to the maintenance of cell homeostasis, under various conditions including high salinity.

The structure and function of chaperonins have been well studied in *Escherichia coli*, GroEL that comprises identical subunits of tetradecamer GroEL (referred to as Tcpn60 in *T. halophila*, formerly GroEL in Ref. 3) and heptamer GroES (Tcpn10 in *T. halophila*, formerly GroES in Ref. 3). The tetradecamer GroEL consists of two heptameric rings stacked back to back on top of each other (9, 10). The GroEL complex forms a cylinder and makes an interior dome cavity with a lid-like component of the GroES complex, which affords an important space for the chaperonin function (11).

In order to study the function of chaperonins, it is indispensable to obtain the correct form of the chaperonin oligomeric complex, which is the tetradecamer core moiety of the cpn60 cylinder as a minimum unit with chaperonin activity. In the present study, we realized the reassembly of recombinant *T. halophila* cpn60 (Tcpn60) to the tetradecamer cylindrical complex showing ATPase and refolding activities under a wide range of salt concentrations. The functionality of Tcpn60 was also examined together with that of Tcpn10 *in vivo* by heterologous expression in *E. coli*.

* Corresponding author. e-mail: sonomoto@agr.kyushu-u.ac.jp
phone/fax: +81-(0)92-642-3019

MATERIALS AND METHODS

Plasmids and strains *E. coli* strains used in this study are listed in Table 1. To construct plasmid pET-CPN60, the Tcpn60 gene was amplified from genomic DNA isolated from *T. halophila* JCM5888 by PCR with a set of primers, Tcpn60-F (5′-TCAGAAGCATATGGCAAAAGATATTAAATTTTCAG-3′) and Tcpn60-R (5′-TCGCTCGCTCGAGTACTGTTCA-3′). For pET-CPNS, a fragment corresponding to the Tcpn10-Tcpn60 operon was amplified with the primers, Tcpn10-f (5′-TTGGAGGGACATATGGTGTTAAAACCATTA-3′) and Tcpn60-R. Each PCR product was digested by *Nde*I and *Xho*I and ligated into the pET-14b expression vector (Novagen, Madison, WI, USA) treated with the same restriction enzymes. The resultant plasmids were transformed into *E. coli* BL21(DE3) (Novagen).

Expression of Tcpn60 gene in *E. coli* *E. coli* TH-CPN60 was grown at 37°C in 2×YT medium (1.6% tryptone, 0.5% yeast extract and 0.5% NaCl) supplemented with 50 μg/ml ampicillin. When the absorbance at 600 nm of the culture reached 0.5–0.6, isopropyl-1-thio-β-D-galactopyranoside (IPTG) was added to final concentration of 1 mM. After additional incubation for 3 h at 37°C, the cell pellets were harvested by centrifugation at 9000×*g* for 20 min and stored at −80°C.

Purification of recombinant Tcpn60 The cell pellets were resuspended in 2 volumes of 20 mM Tris–HCl (pH 7.4) containing 10 mM imidazole, 500 mM NaCl, 1 mM PMSF and 10 μg/ml leupeptin. After sonication, cell debris was removed by centrifugation at 9000×*g*, the supernatant was loaded onto a nickel affinity column (Amersham Pharmacia Biotech, Uppsala, Sweden) and the column was subsequently washed with 10 ml each of the following buffers: 20 mM Tris–HCl (pH 7.4), 10 mM imidazole, 500 mM NaCl; 20 mM Tris–HCl (pH 7.4), 10 mM imidazole, 200 mM KCl, 2 mM ATP, 5 mM $MgCl_2$; 20 mM Tris–HCl (pH 7.4), 30 mM imidazole, 500 mM NaCl. In the washing step, MgATP was added to remove any bacterial DnaK bound to the recombinant Tcpn60 (12). The proteins bound to the column were eluted with 20 mM Tris–HCl (pH 7.4) containing 500 mM NaCl and 500 mM imidazole. Fractions containing His_6-tagged Tcpn60 were pooled and applied to a Sephadex G-50 (Amersham Pharmacia Biotech) column (1×15 cm) or dialyzed with Slide A-lyzer cassette (Pierce, Rockford, IL, USA) in 50 mM Tris–HCl (pH 7.4), 10 mM $MgCl_2$ and 100 mM NaCl (buffer A) and then concentrated by ultrafiltration (Millipore, Bedford, MA, USA). The concentrated sample of His_6-tagged Tcpn60 was then applied to a TSK G4000SW_{XL} gel filtration column (7.8 mm, inner diameter×30 cm; Tosoh, Tokyo) equilibrated with buffer A. The column was developed by the same buffer at flow rate of 0.5 ml/min and monitored by ultraviolet absorption at 280 nm. The maximum volume injected was 100 μl. Fractions (0.5 ml each) containing monomeric Tcpn60 were collected and concentrated to >32 μM by ultrafiltration (Millipore) for subsequent use in the reconstitution experiment.

Reconstitution of Tcpn60 Reconstitution experiments of the Tcpn60 monomer into the oligomer were performed according to the methods previously reported (13–15) with some modifications. Briefly, the concentrated monomeric Tcpn60 (>32 μM protomer) was mixed with a solution containing Tris–HCl (pH 7.4), $MgCl_2$ and ATP so that the final concentrations were 50 mM, 10 mM and 2 mM, respectively. Then, ammonium sulfate was added gradually to the monomeric cpn60 solution to a final concentration of 800 mM and the mixture incubated for 60 min to promote reassembly of Tcpn60. Additional ammonium sulfate was then added to be 60% saturation to precipitate the oligomer. After centrifugation, the Tcpn60 oligomer pellet was dissolved in 50 mM Tris–HCl (pH 7.4), 10 mM $MgCl_2$, 100 mM NaCl and 0.2 mM ATP (buffer B). Then, the reconstituted oligomers were isolated by TSK G4000SW_{XL} gel filtration column chromatography at a flow rate of 0.5 ml/min with buffer B.

Determination of native molecular weight The native molecular weight of the Tcpn60 was determined by TSK G4000SW_{XL} gel filtration column chromatography at a flow rate of 0.5 ml/min with a molecular weight standards kit (Sigma, St. Louis, MO, USA) including thyroglobulin (669,000), apoferritin (440,000), alcohol dehydrogenase (150,000) and carbonic anhydrase (29,000).

Electron microscopy The morphology of the reconstituted Tcpn60 was examined by negative-staining using 0.5% uranyl acetate in a JEM 2000EX electron microscope (JEOL, Tokyo) at 100 kV.

Secondary structure of the recombinant Tcpn60 The purified Tcpn60 oligomer (4.1 μM protomer) and monomer (3.6 μM protomer) were dialyzed against 50 mM Tris–HCl (pH 7.5) and analyzed with a JASCO J-720 spectropolarimeter (JASCO, Tokyo) using a cuvette with a path length of 0.1 cm (far-UV) at 25°C. Ellipticity was measured from 200 to 250 nm at 1-nm intervals, corrected for buffer base lines and converted to molar ellipticity (θ) that is expressed as $deg \cdot cm^2 \cdot dmol^{-1}$.

ATPase activity The ATPase activity of Tcpn60 was measured by quantitation of Pi released from ATP using a modified malachite green assay (16). The assay mixture contained 50 mM Tris–HCl (pH 7.5), 10 mM $MgCl_2$, 2 mM ATP, 50 mM KCl and 36 μg of the purified Tcpn60 oligomer and monomer. The reactions were terminated by the addition of perchloric acid after incubations at 30°C for 0, 10, 20 and 30 min. The samples were put on ice and centrifuged briefly. The inorganic phosphate produced by ATP hydrolysis was quantitated by mixing the sample with malachite green and ammonium molybdate solution followed by measuring the absorbance at 620 nm using 96-well microplates. All data presented were corrected for spontaneous ATP hydrolysis under the conditions tested.

Salt requirement for Tcpn60 ATPase activity To determine the salt-dependence of Tcpn60 ATPase activity, Tcpn60 was added to 50 mM Tris–HCl, pH 7.5, containing 10 mM $MgCl_2$ and 50 mM KCl at 30°C and supplemented with various salts as indicated in the legend of Fig. 5. Activity at 10 mM $MgCl_2$ and 50 mM KCl is set to 100%.

Refolding assay of guanidine–HCl denatured enolase Yeast enolase (26 μM; Sigma) was denatured with 8 M guanidine–HCl (Gdn–HCl) and 2 mM DTT in 50 mM Tris–HCl (pH 7.5) at 30°C for 30 min. The denatured enolase was rapidly diluted with 50 mM Tris–HCl (pH 7.5) containing 10 mM Mg acetate, 20 mM KCl and 2 mM DTT so that the final concentrations of enolase and Gdn–HCl were 0.2 μM and 60 mM, respectively, in the absence and presence of the indicated concentration of NaCl. Refolding of the denatured enzyme was done at 30°C with the reconstituted Tcpn60 tetradecamer and ATP at the respective final concentrations of 0.4 μM and 2 mM. The final volume of the refolding mixture was 500 μl. The activity of the refolded enolase was measured

TABLE 1. *E. coli* strains used in this study

Strain	Genotype	Source
BL21(DE3)	*F⁻, ompT, hsdS*$_B$($r_B^-m_B^-$) *gal, dcm* (DE3)	Novagen
PET14	BL21(DE3) carrying pET14b (*amp*)	This study
TH-CPN60	BL21(DE3) carrying pET-CPN60 (*amp, cpn60*)	This study
TH-CPNS	BL21(DE3) carrying pET-CPNS (*amp, cpn10, cpn60*)	This study

as described below, and the refolding efficiency was evaluated as the specific activity of refolded enolase relative to that of untreated enolase.

Reactivation of thermally inactivated enolase Yeast enolase (Sigma) was thermally inactivated at 53°C for 30 min in 50 mM Tris–HCl (pH 7.5) containing 10 mM $MgCl_2$ and 20 mM KCl. Reactivation was examined at 30°C by diluting the inactivated enolase with 50 mM Tris–HCl (pH 7.5) containing 10 mM $MgCl_2$, 20 mM KCl and 2 mM DTT in the presence and absence of the reconstituted Tcpn60 tetradecamer of 0.4 μM. ATP was added to a final concentration of 2 mM. The final volume of the reaction mixture was 500 μl. The activity of the reactivated enolase was measured, and the reactivation efficiency was evaluated as the specific activity of reactivated enolase as a percentage of that of enolase before inactivation.

Measurement of enolase activity The activity of enolase was measured at 25°C using 2-phosphoglycerate (2-PGA) as the substrate (17). The enzyme solution (40 μl) was mixed with 0.96 ml of substrate solution (1 mM 2-PGA in 50 mM Tris–HCl [pH 7.5] and 1 mM $MgCl_2$). The activity was determined as the increase in absorbance at 240 nm as a function of time.

Growth of recombinant *E. coli* under high stress conditions A single colony of *E. coli* PET14, TH-CPN60, or TH-CPNS was inoculated into 20 ml of LB medium containing 20 μg/ml of ampicillin at 37°C overnight. The pre-cultures were then diluted into 200 ml of LB broth containing 1 mM IPTG, 200 μg/ml ampicillin and 0.86 M NaCl and incubated at 37°C in shaking incubator. Cell growth was measured at OD_{600}.

Other methods Proteins were analyzed by polyacrylamide gel electrophoresis either in a 9% polyacrylamide gel containing 0.1% SDS or in a 6% polyacrylamide gel without SDS. Gels were stained by Coomassie Brilliant Blue (18). Protein concentration was determined by the method of Bradford (19) with bovine serum albumin as a standard.

RESULTS

Cloning and overexpression of Tcpn60 in *E. coli* Tcpn60 was overexpressed in *E. coli* as His_6-tagged fusion proteins. SDS–PAGE analysis of the cell extract from *E. coli* TH-CPN60 showed an IPTG-induced major band at the 62-kDa position after IPTG induction which was not detected in the cell extracts of *E. coli* PET14. It was suggested that the 62-kDa band represented His_6-tagged Tcpn60 since its molecular size was in agreement with the molecular mass calculated from the deduced amino acid sequence of the His_6 fusion protein.

Purification and reconstitution of oligomeric recombinant Tcpn60 The fusion protein of Tcpn60 with the N-terminal His_6-tag was partially purified by nickel affinity chromatography. Since SDS–PAGE of the fraction purified by affinity chromatography showed some impurities, gel filtration column chromatography with TSK G4000SW$_{XL}$ was used as an additional purification step and yielded the Tcpn60 protein showing a single band upon SDS–PAGE (Fig. 1A, inset). The retention time in the gel filtration chromatography revealed that the molecular size of the recombinant Tcpn60 corresponded to the monomer instead of the oligomer.

Reconstitution of the Tcpn60 oligomer was first attempted using Mg^{2+} and MgATP. However, a major shift in the apparent molecular size was not detected in the gel filtration chromatography analyses (Fig. 1A). Thus ammonium sulfate was then added stepwise to the solution previously supplemented with $MgCl_2$ and ATP to a final concentration of 800 mM. Further additional ammonium sulfate was added to 60% saturation to precipitate the Tcpn60 protein. Then, the reconstituted Tcpn60 solution was applied onto a TSK G4000SW$_{XL}$ gel filtration column. As shown in Fig. 1B, two distinct peaks were observed. The first peak was eluted before thyroglobulin, indicating that this protein was eluted as a large oligomeric complex, while a second peak corresponded to the original monomer. SDS–PAGE analysis revealed that both peaks contained a 62-kDa protein subunit of Tcpn60 (Fig. 1B, inset).

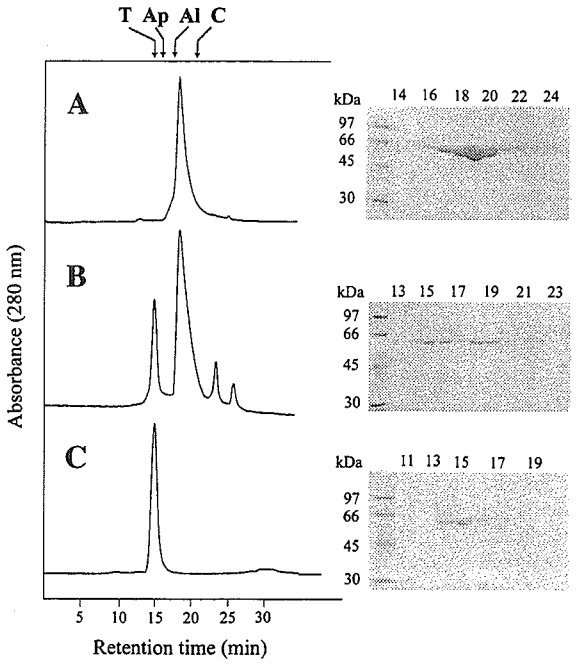

FIG. 1. Gel filtration chromatography profiles of the recombinant Tcpn60 upon TSK G4000SW$_{XL}$ gel filtration chromatography followed by SDS–PAGE analysis of fractions (inset). (A) Purified recombinant Tcpn60 monomer. (B) Tcpn60 after incubation with MgATP and ammonium sulfate. (C) Rechromatography of the peak at 15 min in panel B. Protein elution was monitored by absorption at 280 nm. The arrows indicate the elution position of standard proteins: thyroglobulin (T, 669 kDa), apoferritin (Ap, 440 kDa), alcohol dehydrogenase (Al, 150 kDa) and carbonic anhydrase (C, 29 kDa). The numbers at the top of the SDS–polyacrylamide gels indicate the retention time (min) of fractions from the gel filtration chromatography.

The first peak was collected and then concentrated to 6.4 μM by ultrafiltration. The apparent molecular size was determined to range from 800 to 880 kDa, by second round gel filtration chromatography (Fig. 1C) that is nearly identical to the theoretical molecular size of the tetradecamer. The protein band of these fractions contained a 62-kDa protein subunit of Tcpn60 (Fig. 1C, inset). The reconstituted oligomer was further analyzed by 6% native PAGE and migrated aberrantly slower than that of the monomeric fraction. This coincided with the result of gel filtration and suggested that the Tcpn60 oligomer was obtained.

Electron micrograph of the reconstituted Tcpn60 oligomer Electron microscopy of the reconstituted cpn60 oligomer revealed a number of particles with two types of

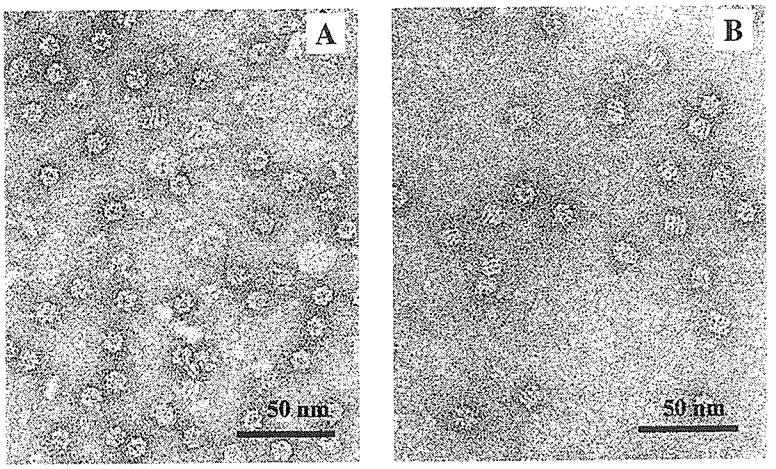

FIG. 2. Electron micrograph of the reconstituted Tcpn60 oligomer. (A) Top view of the Tcpn60 oligomer displaying the ring shape. (B) Side view of the Tcpn60 oligomer displaying the rectangular shape. The scale bar represents 50 nm.

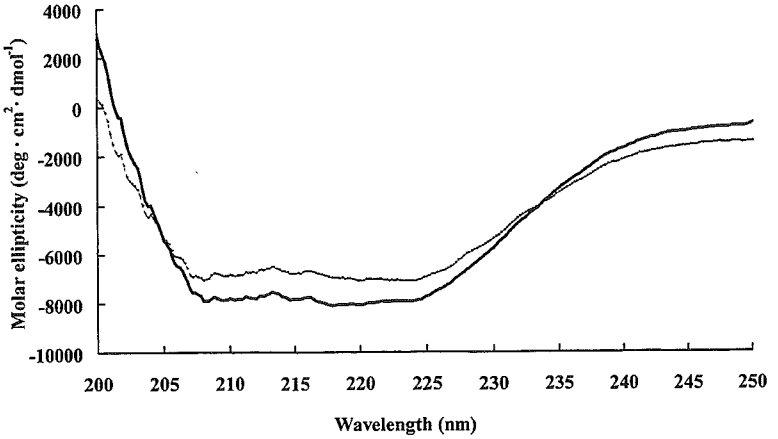

FIG. 3. The circular dichroism of the recombinant Tcpn60 tetradecamer (thick line) and monomer (thin line). The respective protein concentrations of the tetradecamer and monomer were 4.1 μM and 3.6 μM as protomer concentrations. The path length and the resolution were 0.1 cm and 0.2 nm, respectively. Spectra were measured four times and averaged.

forms showing toroidal (Fig. 2A) and rectangular structures (Fig. 2B). Careful observation revealed that the toroidal ring consisted of seven small subunits and the rectangle consisted of four stripes. These images correspond to typical top and side views of the chaperonin core complex, respectively, which represent the well-known double toroidal tetradecamer structure of natural chloroplast and bacterial cpn60.

Secondary structure of the Tcpn60 tetradecamer and monomer The secondary structure of the Tcpn60 tetradecamer and monomer was analyzed by circular dichroism (CD) spectroscopy in the far-UV from 200 to 250 nm (Fig. 3). Both CD spectra displayed the double minimum of the transitions at 208 and 222 nm, characteristics of α-helices. The helix contents of the tetradecamer and monomer estimated by the ellipticity were almost identical, suggesting no significant change in secondary structure during the *in vitro* reconstitution reaction.

ATPase activity of the Tcpn60 tetradecamer and monomer The ATPase activity of the reconstituted Tcpn60 tetradecamer was measured and compared with that of the monomer (Fig. 4). The ATPase activity of the reconstituted oligomer was about eight times higher than that of the monomer, suggesting that Tcpn60 functioned in the tetradecameric form. No significant ATPase activity was observed in the absence of $MgCl_2$, indicating that magnesium is essential for the ATPase activity. Thus, the subsequent experiments were performed using 10 mM $MgCl_2$. The ATPase activity was measured under various concentrations of KCl and NaCl (Fig. 5). The activity increased markedly in the presence of KCl and remained stable up to 1 M, the highest concentration in this test. On the other hand, NaCl did not promote the ATPase activity, which decreased gradually with increasing NaCl concentration. The ATPase activity was also measured at various concentrations of NaCl and a constant KCl concentration (50 mM). As a result, the activity decreased with increasing NaCl concentration higher than 50 mM.

Refolding activity of the reconstituted Tcpn60 tetradecamer The refolding activity of the reconstituted Tcpn60 tetradecamer was analyzed using chemically and

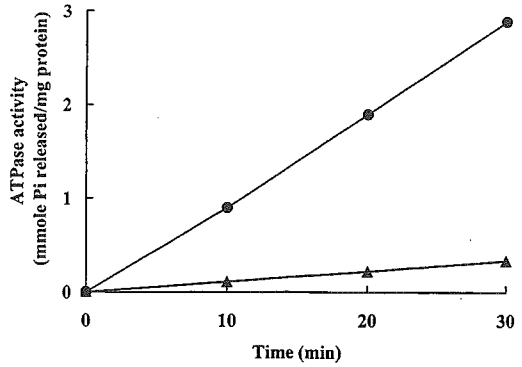

FIG. 4. ATPase activity of the recombinant Tcpn60 tetradecamer (circles) and monomer (triangles). The assay mixture contained 50 mM Tris–HCl (pH 7.5), 10 mM $MgCl_2$, 2 mM ATP, 50 mM KCl and 36 μg of the purified Tcpn60 tetradecamer and monomer.

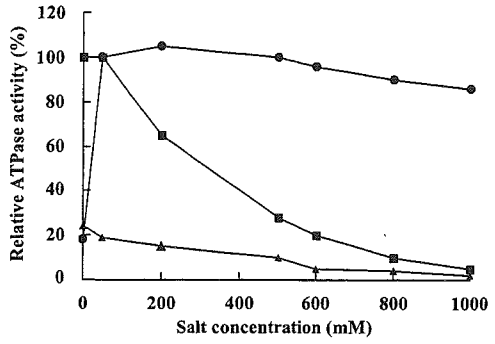

FIG. 5. ATPase activity of Tcpn60 under various salt concentrations. The Tcpn60 tetradecamer was supplemented with various salts as indicated below. The recombinant Tcpn60 was incubated in 50 mM Tris–HCl buffer pH 7.5 with 10 mM $MgCl_2$ with increasing KCl concentrations (circles), NaCl (triangles) and NaCl in the presence of 50 mM KCl (squares). ATPase activity at 10 mM $MgCl_2$ and 50 mM KCl was set to 100%.

thermally denatured enolases as substrates. The chemically denatured enolase spontaneously recovered up to about 60–70% of its initial activity. In the presence of ATP (2 mM) and the Tcpn60 tetradecamer (0.4 μM), enolase activity was recovered to 86%, suggesting the refolding activity of the reconstituted Tcpn60 tetradecamer (Fig. 6). Incubation of enolase at 53°C for 30 min decreased its activity to less than 30%. Figure 7 shows the reactivation of thermally inactivated enolase by Tcpn60 in the presence of ATP. The thermally denatured enolase was gradually reactivated, while no recovery of its activity was observed in the absence of chaperonin. The refolding activity was measured under various concentrations of NaCl (Fig. 8). The activity decreased with increasing NaCl concentration but significant activity was detected at 1.2 M NaCl, the highest concentration in this experiment.

Effect of heterologous expression of Tcpn60 and Tcpn10 on growth under salt stress conditions The effect of the heterologous expression of Tcpn60 and Tcpn10 in *E. coli* on the growth under salt stress conditions was examined (Fig. 9). The growth of strain PET14 (vector control) exhibited a very long lag phase of about 12 h under 5%

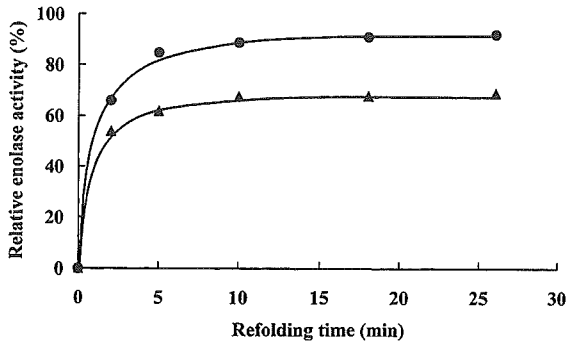

FIG. 6. Time course of refolding of Gdn–HCl-denatured enolase in the presence (circles) and absence (triangles) of the reconstituted Tcpn60 tetradecamer (0.4 μM) and 2 mM ATP at 30°C. The activity of the refolded enolase was measured and the refolding efficiency was evaluated as the specific activity of refolded enolase relative to that of untreated enolase.

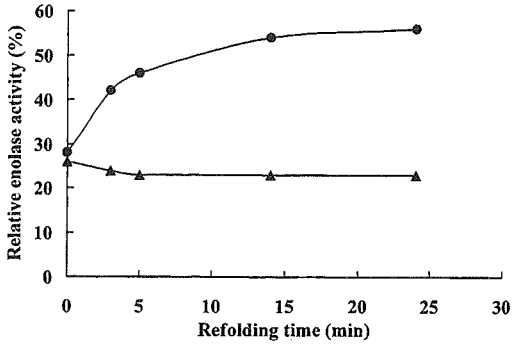

FIG. 7. Time course of refolding of thermally inactivated enolase in the presence (circles) and absence (triangles) of the reconstituted Tcpn60 tetradecamer (0.4 μM) and 2 mM ATP at 30°C. The enzyme concentration was 0.2 μM. The activity of the reactivated enolase was measured, and the reactivation efficiency was evaluated as the specific activity of reactivated enolase as a percentage of that of enolase before inactivation.

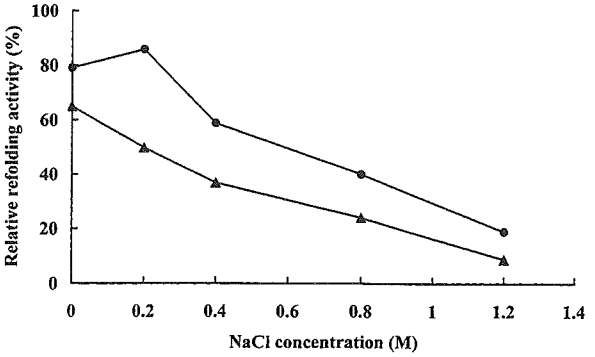

FIG. 8. The effect of various NaCl concentrations in the refolding of Gdn–HCl-denatured enolase with Tcpn60. Refolding was assayed 10 min after dilution as measured by the increasing absorbance at 240 nm, ΔA_{240}/min for 0.2 μM of native enolase corresponding to 100% refolding. Results are expressed as the relative percentage of refolding activity. Refolding in the absence of chaperonin (triangles); refolding in the presence of reconstituted Tcpn60 and 2 mM ATP (circles).

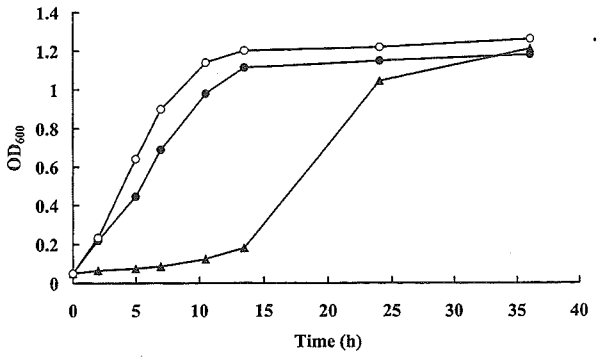

FIG. 9. Time course of cell growth of the recombinant *E. coli* PET14, TH-CPN60 and TH-CPNS in LB medium containing 5% (0.86 M) NaCl. Overnight cultures of the bacteria grown at 37°C in Luria–Bertani medium were diluted to an optical density at 600 nm (OD_{600}) of 0.05. Cultivation of strain TH-CPN60 (closed circles), TH-CPNS (open circles) and PET14 (triangles) was carried out in a shaking incubator at 37°C. Aliquots were removed at various time intervals to measure cell density (OD_{600}).

NaCl. As observed in *E. coli* TH-CPN60, expression of Tcpn60 shortened the prolonged lag-phase to the level of normal lag-phase observed under non-stress conditions. As observed in *E. coli* TH-CPNS, co-expression of Tcpn60 and Tcpn10 showed a higher promotive effect on the growth. These results suggested that the expression of Tcp60 enabled the *E. coli* cells to rapidly adapt to the salt stress conditions and the efficiency was higher when expressed together with Tcpn10.

DISCUSSION

There is little available information about the oligomeric form of moderately halophilic cpn60 or lactic acid bacteria cpn60. There is only one report of the moderately halophilic *Pseudomomas* sp. #43 in which the purified GroEL was observed as various oligomeric forms which partially dissociated to the monomeric form during electrophoresis (20). In this study, the gel filtration chromatography analysis (Fig. 1A) and native PAGE analysis indicated that Tcpn60 expressed in *E. coli* existed in the monomeric form rather than the expected natural form of the tetradecamer. The CD spectrum showed that the Tcpn60 monomer was correctly folded as well as the reconstituted cpn60 oligomer (Fig. 3). However, the *E. coli*-expressed Tcpn60 could not form the oligomer spontaneously. This suggested that the lack of oligomerization was not due to misfolding of the monomer Tcpn60 subunit.

The lack of the oligomer may be due to the dissociation of the oligomer during the extraction or purification step as observed in *Pseudomonas* sp. #43 (20), mammalian mitochondrial chaperonin 60 (21), *Thermus thermophilus* HB8 (22), and *Thermoanaerobacter brockii* (23). At present, it is difficult to determine why the recombinant Tcpn60 oligomeric form was unstable and spontaneously dissociated into the monomeric form during the purification step. One possible reason for the dissociation of the Tcpn60 oligomer might be the release of nucleotides (15). It has been reported that the *in vitro* reconstitution of some cpn60s from various microorganisms is achieved in the presence of MgATP or MgATP with ammonium sulfate (13–15). Based on these previous studies, we performed the reconstitution to obtain the functional oligomer in the same manner. After various attempts using reconstitution methods in which ammonium sulfate was added to the cpn60 solution containing MgATP with some modifications (14), we finally obtained the reconstituted Tcpn60 oligomer showing the well-known double toroidal, tetradecameric structure of the bacterial chaperonin core complex upon electron microscopy (Fig. 2). However, even after the reconstitution reaction, a major fraction of Tcpn60 still remained as the monomer as shown by the gel filtration (Fig. 1B), suggesting that another factor may be required to increase the yield of the oligomer. Structural cooperation with the co-chaperonin (Tcpn10) complex may also be important as found in the natural form of chaperonin complex.

The tetradecamer Tcpn60 complex showed much higher ATPase activity than the monomer (Fig. 4), although each subunit contains an ATP binding site. This agrees with some previous studies such as that on *E. coli* GroEL (13) or *Mycobacterium tuberculosis* GroEL (24) and suggests that the quarternary structure of cpn60 is very important for the ATPase activity. The effects of salts on the ATPase activity of the Tcpn60 tetradecamer were examined in detail (Fig. 5). Tcpn60 exhibited no ATPase activity in the absence of magnesium ions. The requirement for magnesium ions for the ATPase activity has been reported to involve coordination of the nucleotide as the cofactor to facilitate the hydrolysis of ATP by cpn60 (25). Potassium ions also markedly enhanced the ATPase activity of Tcpn60 and the activity was maintained up to 1 M potassium chloride, which the maximum concentration used in this experiment. On the contrary, the ATPase activity decreased with increasing sodium chloride concentration. Furthermore, in the presence of potassium ions, sodium ions showed an antagonistic effect on the activation of Tcpn60 ATPase activity by potassium ions. These halophilic properties of Tcpn60 ATPase activity may reflect a bioenergetic aspect of the halophile in which potassium ions are accumulated inside the cell instead of sodium ions (26). The inhibitory and antagonistic effects of sodium ions have been found for chaperonins from other halophiles, *e.g.*, *Pseudomonas* sp. #43 (20) and *Haloferax volcanii* (27).

Under low salt condition, the reconstituted Tcpn60 tetradecamer not only enhanced the refolding rate of the chemically denatured enolase, but also reactivated the thermally inactivated enolase to over 50% of its initial activity. In efforts to elucidate the mechanism by which the protein is refolded, significant differences between chemically and thermally denatured enolases have already been reported. It was suggested that the thermal denaturation process of enolase is irreversible, whereas the chemically denatured enolase is in dynamic and various unfolded states and has native secondary structure which can be disrupted (28–30). Our result is consistent with that observation. The activity of chemically denatured enolase used for this refolding assay spontaneously recovered from 0% to more than 60% of its initial activity within 5 min. On the other hand, heat-denatured enolase did not show any recovery of activity greater than 25% of the initial activity. These results imply that a

major fraction of the chemically denatured enolase was in the reversible state which can be refolded to the natural form, whereas the heat treatment changed the enolase molecule into the irreversibly-denatured form. The refolding of chemically denatured enolase by Tcpn60 was decreased significantly with increasing NaCl concentration. Another factor, *e.g.*, Tcpn10, may be required to function efficiently as a molecular chaperone under high salinity conditions.

The contribution of Tcpn60 to salinity adaptation was also observed *in vivo* by the heterologous expression system of the Tcpn60 gene in *E. coli* (Fig. 9). Overexpression of the Tcpn60 gene enabled the host cell to rapidly adapt to the salt stress condition and the effect was increased by co-expression with Tcpn10. This suggested that the *T. halophila* chaperonin proteins actually contribute to maintenance of the native state of various proteins in the cell growing under salt stress conditions. The same type of effect has been observed in *E. coli* transformed with the *T. halophila* molecular chaperone DnaK (5).

In order to gain a better understanding the role of the chaperonins in relation to salinity stress tolerance, further studies with the reconstituted Tcpn10 complex should be necessary. Substrate specificity of Tcpn60 would also be examined both *in vitro* and *in vivo*. This knowledge should shed light on the function of chaperonins in the moderately halophilic and halotolerant lactic acid bacteria.

ACKNOWLEDGMENTS

The authors are grateful to Mr. Akemi Takade (Department of Bacteriology, Faculty of Medical Sciences, Graduate School, Kyushu University, Fukuoka) for the electron microscopy. This work was supported by the Monbusho Scholarship and JSPS Research Fellowships for young scientists.

REFERENCES

1. **Röling, W. F. and Van Verserveld, H. W.:** Characterization of *Tetragenococcus halophila* populations in Indonesian soy mash (kecap) fermentation. Appl. Environ. Microbiol., **62**, 1203–1207 (1996).
2. **Robert, H., Marrec, C. L., Blanco, C., and Jebbar, M.:** Glycine betaine, carnitine, choline enhance salinity tolerance and prevent the accumulation of sodium to a level inhibiting growth of *Tetragenococcus halophila*. Appl. Environ. Microbiol., **66**, 509–517 (2000).
3. **Fukuda, D., Watanabe, M., Aso, Y., Sonomoto, K., and Ishizaki, A.:** The *groESL* operon of the halophilic lactic acid bacterium *Tetragenococcus halophila*. Biosci. Biotechnol. Biochem., **66**, 1176–1180 (2002).
4. **Fukuda, D., Watanabe, M., Sonezaki, S., Sugimoto, S., Sonomoto, K., and Ishizaki, A.:** Molecular characterization and regulatory analysis of dnaK operon of halophilic lactic acid bacterium *Tetragenococcus halophila*. J. Biosci. Bioeng., **93**, 388–394 (2002).
5. **Sugimoto, S., Nakayama, J., Fukuda, D., Sonezaki, S., Watanabe, M., Tosukhowong, A., and Sonomoto, K.:** Effect of heterologous expression of molecular chaperone DnaK from *Tetragenococcus halophilus* on salinity adaption of *Escherichia coli*. J. Biosci. Bioeng., **96**, 129–133 (2003).
6. **Wheelis, M. L., Kandler, O., and Woese, C. R.:** On the nature of global classification. Proc. Natl. Acad. Sci. USA, **89**, 2930–2934 (1990).
7. **Frydman, J., Nimmesgern, E., Ohtsuka, K., and Hartl, F. U.:** Folding of nascent polypeptide chains in a high molecular mass assembly with molecular chaperones. Nature, **370**, 111–117 (1994).
8. **Ellis, R. J. and Van der Vies, S. M.:** Molecular chaperones. Annu. Rev. Biochem., **60**, 321–347 (1991).
9. **Braig, K., Otwinowski, Z., Hegde, R., Boisvert, D. C., Joachimiak, A., Horwich, A. L., and Sigler, P. B.:** The crystal-structure of the bacterial chaperonin GroEL at 2.8 Å. Nature, **371**, 578–586 (1994).
10. **Saibil, H. R., Zheng, D., Roseman, A. M., Hunter, A. S., Watson, G. M. F., Chen, S., auf der Mauer, A., O'Hara, B. P., Wood, S. P., Mann, N. H., Barnett, L. K., and Ellis, R. J.:** ATP induces large quaternary rearrangements in a cage-like chaperonin structure. Curr. Biol., **3**, 265–273 (1993).
11. **Xu, Z. H., Horwich, A. L., and Sigler, P. B.:** The crystal structure of the asymmetric GroEL-GroES-(ADP)7 chaperonin complex. Nature, **388**, 741–750 (1997).
12. **Chamberlain, L. H., and Burgoyne, R. D.:** Activation of the ATPase activity of heat-shock proteins Hsc70/Hsp70 by cysteine-string protein. Biochem. J., **322**, 853–858 (1997).
13. **Ybarra, J. and Horowitz, P. M.:** Inactive GroEL monomers can be isolated and reassembled to functional tetradecamers that contain few bound peptides. J. Biol. Chem., **270**, 22962–22967 (1995).
14. **Furutani, M., Iida, T., Yoshida, T., and Maruyama, T.:** Group II chaperonin in a thermophilic methanogen, *Methanococcus thermolithotrophicus* chaperone activity and filament-forming ability. J. Biol. Chem., **273**, 28399–28407 (1998).
15. **Lissin, N. M., Venyaminov, S. Y., and Girshovich, A. S.:** (Mg-ATP)-dependent self-assembly of molecular chaperone GroEL. Nature, **348**, 339–342 (1990).
16. **Lanzenta, P. A., Alvarez, L. J., Reinach, P. S., and Candia, O. A.:** An improved assay for nanomole amounts of inorganic phosphate. Anal. Biochem., **100**, 95–97 (1979).
17. **Border, C. L., Woodall, M. L., and George, A. L., Jr.:** Essential arginyl residues in yeast enolase. Biochem. Biophys. Res. Commun., **82**, 901–906 (1978).
18. **Laemmli, U. K.:** Cleavage of structural proteins during the assembly of the head of bacteriophage T4. Nature, **277**, 680–685 (1970).
19. **Bradford, M.:** A rapid and sensitive method for the quantitation of microgram quantities of protein utilizing the principle of protein-dye binding. Anal. Biochem., **72**, 248–254 (1976).
20. **Tokunaga, M., Miyawaki, H., Shiraishi, Y., and Tokunaga, H.:** Purification and characterization of a GroEL homologue from the moderately eubacterial halophile *Pseudomonas* sp. #43. FEMS Microbiol. Lett., **152**, 321–326 (1997).
21. **Viitanen, P. V., Lorimer, G., Bergmeier, W., Weiss, C., Kessel, M., and Goloubinoff, P.:** Purification of mammalian mitochondrial chaperonin 60 through *in vitro* reconstitution of active oligomers. Methods Enzymol., **290**, 203–217 (1998).
22. **Amada, K., Yohda, M., Odaka, M., Endo, I., Ishii, N., Taguchi, H., and Yoshida, M.:** Molecular cloning, expression, and characterization of chaperonin-60 and chaperonin-10 from a thermophilic bacterium, *Thermus thermophilus* HB8. J. Biochem., **118**, 347–354 (1995).
23. **Truscott, K. N., Hoj, P. B., and Scopes, R. K.:** Purification and characterization of chaperonin 60 and chaperonin 10 from the anaerobic thermophile *Thermoanaerobacter brockii*. Eur. J. Biochem., **222**, 277–284 (1994).
24. **Qamra, R., Srinivas, V., and Mande, S. C.:** *Mycobacterium tuberculosis* GroEL homologues unusually exist as lower oligomers and retain the ability to suppress aggregation of substrate proteins. J. Mol. Biol., **342**, 605–617 (2004).
25. **Guagliardi, A., Cerchia, L., and Baumeister, W.:** ATPase

cycle of an archaeal chaperonin. J. Mol. Biol., **300**, 187–196 (2000).
26. **Oren, A.:** Bioenergetic aspects of halophilism. Microbiol. Mol. Biol. Rev., **63**, 334–348 (1999).
27. **Large, A. T., Kovacs, E., and Lund, P. A.:** Properties of the chaperonin complex from the halophilic archaeon *Haloferax volcanii*. FEBS Lett., **532**, 309–312 (2002).
28. **Teshima, T., Kondo, A., and Fukuda, H.:** Reactivation of thermally inactivated enzymes by free and immobilized chaperonin GroEL/ES. Appl. Microbiol. Biotechnol., **48**, 41–46 (1997).
29. **Teshima, T., Mashimo, S., Kondo, A., and Fukuda, H.:** Affinity purification and immobilization of fusion chaperonin GroEL-$(His)_6$ and its utilization to mediate protein refolding. J. Ferment. Bioeng., **86**, 357–362 (1998).
30. **Huang, P. and Dong, A.:** Thermal, chemical and chemothermal denaturation of yeast enolase. Spectroscopy, **17**, 453–467 (2003).

Research Signpost
37/661 (2), Fort P.O., Trivandrum-695 023, Kerala, India

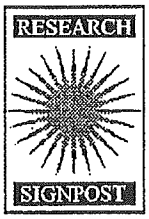

Survival and Death in Bacteria, 2005: 225-246 ISBN: 81-7736-236-4
Editor: Mamoru Yamada

13 Biofilm formation and entry into viable but nonculturable (VBNC) state: Survival strategy under stress conditions

Yoshimitsu Mizunoe[1] and Sun Nyunt Wai[2]
[1]Department of Bacteriology, Faculty of Medical Sciences, Kyushu University Fukuoka 812-8582, Japan; [2]Department of Molecular Biology, Umeå University S-901 87 Umeå, Sweden

Abstract

In nature, bacteria are exposed to many different stressful conditions. Genetic and physiological adaptation of bacterial populations permits survival in environments with rapidly changing conditions. This review presents two aspects of bacterial cells under stressful conditions: biofilm formation and entry into viable but nonculturable (VBNC) state.

Introduction

In the natural environment, bacteria are constantly exposed to variable and stressful conditions. When

Correspondence/Reprint request: Dr. Yoshimitsu Mizunoe, Department of Bacteriology, Faculty of Medical Sciences, Kyushu University, Fukuoka 812-8582, Japan. E-mail: ymizunoe@bact.med.kyushu-u.ac.jp

bacteria are transported from one environment to another, they are confronted by the changes in temperature, nutrient level, salinity, salt condition, pH, and many other factors (1). Many pathogenic and commensal bacteria are capable of transitioning between life in the environment and in the human host, and all must be able to adapt to sudden shifts in nutrient availability as well as to primary and secondary host immune defenses (2). Bacteria have evolved numerous adaptive mechanisms to facilitate their survival under changing environmental conditions. As a response to nutrient depletion, copiotrophic (3, 4), heterotrophic bacteria may undergo considerable morphological, physiological, and chemical changes (5-10). In fact, to survive energy- and nutrient-deprived conditions, non-spore-forming, heterotrophic bacteria are known to undergo an active adaptation program (10).

One such mechanism is phase variation, which occurs when the expression of a given factor is periodically altered such that it is either "on" or "off." These variations are generally spontaneous and reversible and occur at relatively high frequency ($>10^{-5}$ per generation) (11). Factors that are controlled by phase variation are often associated with the cell surface and include structures such as flagella, fimbriae, outer membrane proteins, and exo- and lipopolysaccharide (11). *Vibrio cholerae* can shift to a rugose colony morphology from its normal translucent smooth colony morphology in response to environmental stress including nutrient starvation (12, 13). The rugose strains produce more exopolysaccharide (EPS) than the smooth colony, acquired resistance to osmotic and oxidative stress, and promote biofilm formation (12-14). The similar phenomenon has been observed in *Vibrio parahaemolyticus* strains (15-17). Biofilm formation occurs on virtually any surface in any environment in which bacteria are present. These include natural (18) and industrial (19) ecosystems and infections (20-24). From an ecological standpoint, growth as a biofilm offers survival advantage in bacterial pathogenecity (20, 24-26).

The viable but nonculturable (VBNC) state is also thought to be a survival strategy adopted by bacteria when exposed to hostile environmental stress (1, 27-30). In the VBNC state, bacteria cannot be recovered by standard culture methods, but the cells still display active metabolism (31, 32), respiration (31), membrane integrity (33) and gene transcription with specific mRNA production (34).

In this review, we will discuss the bacterial survival strategy under stress conditions, focusing on biofilm formation of *V. cholerae* and the entry into VBNC state of several pathogenic bacteria.

Biofilm formation

Bacteria predominantly exist in sessile communities rather than as free-living cells. These communities develop as biofilms on all surfaces in aqueous

environments. Biofilm formation is linked to development and differentiation in microorganisms at large, possibly also more broadly to multicellular biological differentiation systems (2). Development is not restricted to so-called higher organisms. Developmental processes in bacteria include differentiation of a single cell, such as the swarmer-to-stalk transition by *Caulobacter crescentus* and spore formation by *Bacillus subtilis.* As we learn more about microbial biofilm formation, it is becoming clear that this is yet another example of a bacterial developmental process (35, 36). Like other developmental systems, building a biofilm requires a series of discrete and well-regulated steps. These stages include attachment of cells to a substrate, the growth and aggregation of cells into microcolonies, and the maturation and maintenance of architecture (37, 38). While the stages of biofilm development appear to be conserved among a wide range of microbes, the exact molecular mechanisms may differ from organism to organism. One such different mechanism has been observed in *V. cholerae* that biofilm formation is associated with phase variation of colony morphology (12-14).

Phase variation of *V. cholerae* in response to stress conditions

V. cholerae is the causative agent of cholera, which in its most severe form is characterized by profuse diarrhea, vomiting, and muscle cramps. *V. cholerae* strains have been divided into two groups, O1 and non-O1, based on their ability to cause cholera epidemics. To date, there have been seven recorded pandemics of this severe dehydrating diarrheal disease caused by *V. cholerae* strains of serotype O1, and it was therefore assumed that only this serotype has epidemic potential. The new serogroup, designated O139 synonym Bengal, is the first recorded serogroup other than O1 to cause epidemic cholera. *V. cholerae* O139 closely resembles *V. cholerae* O1 biotype El Tor strains of the seventh pandemic (39-42). The major differences between *V. cholerae* O139 and O1 are the composition and lengths of the O side chains of the cell wall lipopolysaccharide (LPS) and the presence of a capsular polysaccharide (CPS) in O139 strains that is not found in *V. cholerae* O1 strains (43-45). Serological and genetic studies suggested that CPS of O139 *V. cholerae* has the same repeating unit as the O antigen (46, 47).

We have shown that *V. cholerae* O1 and *V. cholerae* O139 underwent phase variation from smooth colony to rugose colony when incubated at low temperature under starvation (Fig. 1). We found that several other stress conditions including high osmorality, high concentration of antibiotics, acidity and freezing can also convert *V. cholerae* to rugose phase variant. The rugose form of *V. cholerae* was first described in 1938 by Bruce White, who recognized that it might serve as a survival form of the organism (48). Rice et al. (49) suggested that the *V. cholerae* rugose phenotype represents a fully virulent survival form of the organism that can persist in the presence of free

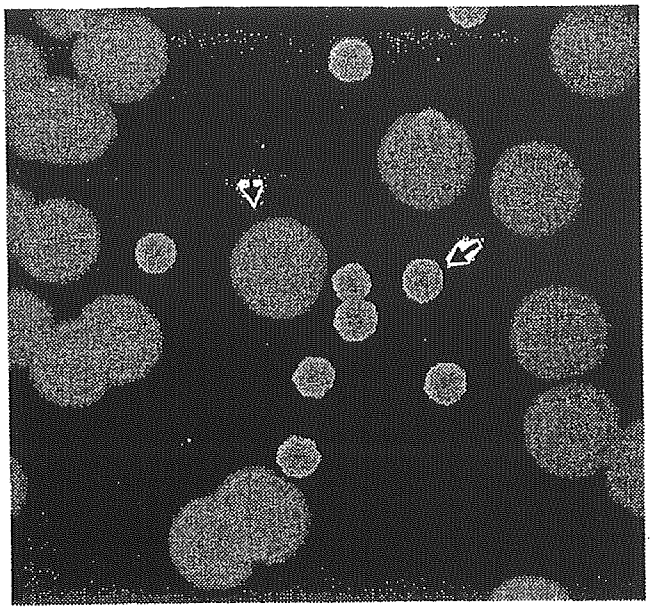

Figure 1. Photomicrograph of *V. cholerae* O139 rugose (arrow) and smooth (arrow head) colonies.

chlorine and that this phenotype may limit the usefulness of chlorination in blocking the endemic and epidemic spread of cholera. Morris et al. (50) subsequently showed that the rugose variant can cause cholera in orally challenged human volunteers and retains its colonial morphology after passage through the human host. More recent studies have shown that epidemic strains of *V. cholerae* switch from the smooth to the rugose phase more frequently than clinical isolates (51), and that this phase transition increases the resistance of the organism to osmotic, oxidative and acidic stress (12-14, 52).

EPS production and biofilm formation by rugose variant of *V. cholerae*

Rugose colony-forming *V. cholerae* O1 produces EPS materials recognized as a heavy, fibrous, electron-dense, ferritin-stained layer surrounding the cells (Fig. 2A), but smooth colony-forming *V. cholerae* O1 did not appear to have this EPS layer surrounding it (Fig. 2B). Like *V. cholerae* O1 rugose strain, *V. cholerae* O139 rugose strain was also shown to produce EPS recognized as heavy electron-dense layer surrounding the cell in addition to a thin electron-dense layer of capsule (Fig. 2C and D). It has been reported that exoploysaccharide (EPS) synthesis is involved in the formation of three-dimensional biofilm architecture in several bacterial species; EPS colanic acid in *Escherichia coli* (53) and EPS alginate in *Pseudomonas aeruginosa* (54, 55).

To determine whether EPS production of *V. cholerae* is related to biofilm formation, *V. cholerae* O1 and O139 rugose variants were cultured overnight

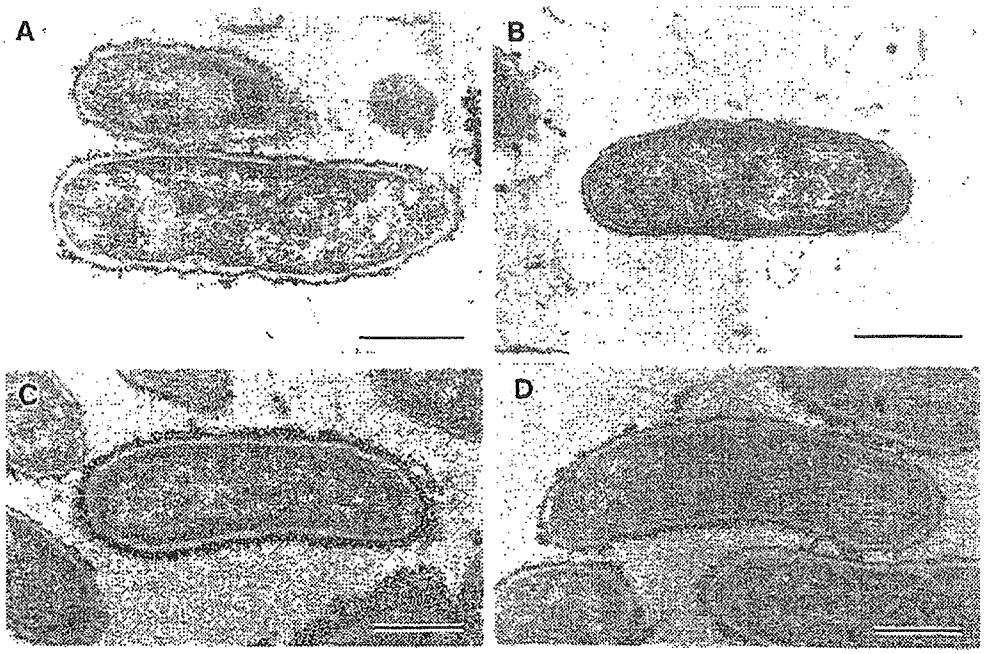

Figure 2. Thin section of *V. cholerae* O1 and O139 stained with polycationic ferritin. O1 rugose strain was surrounded by a thick, electron-dense slime layer (A) and the absence of this layer on O1 smooth strain (B). A thick, electron-dense slime layer in addition to a thin electron-dense layer of capsule on O139 rugose cells (C) and no slime layer on O139 smooth strain (D). Bars, 0.5 μm.

in liquid medium at static condition. We found that rugose variants produced a continuous biofilm on the colonized surface and culture tube walls. The biofilm of rugose variants of *V. cholerae* was clearly visible on the surface of medium and culture tube wall after static incubation, whereas smooth variants did not have the biofilm-forming property and produced a homogenous suspension of bacteria (Fig. 3). Scanning electron microscopic examination revealed that the surface of the biofilm was completely covered with a layer of rod cells embedded within a polymeric matrix (Fig. 4A). Throughout the biofilm, cells were interconnected by a finger-like glycocalyx matrix that extended from the substratum to the outer boundaries of the biofilm. Interestingly, some of the surface of the biofilm was covered by a twisting long filamentous growth of bacteria (Fig. 4B). To investigate the ultrastructural changes of bacteria in biofilm and planktonic counterparts, we sampled biofilm and culture media containing planktonic cells from the same tube after 2 days incubation. Thin-sectioning electron micrographs of *V.cholerae* cells in biofilm revealed the typical rod-shaped cells with a uniform distribution of electron-dense ribosomal and nucleic acid material through out the cytoplasm, seeming to be normal (Fig. 5A). On the other hand, thin-section micrograph of planktonic *V. cholerae* cells from culture media showed that most of cells were

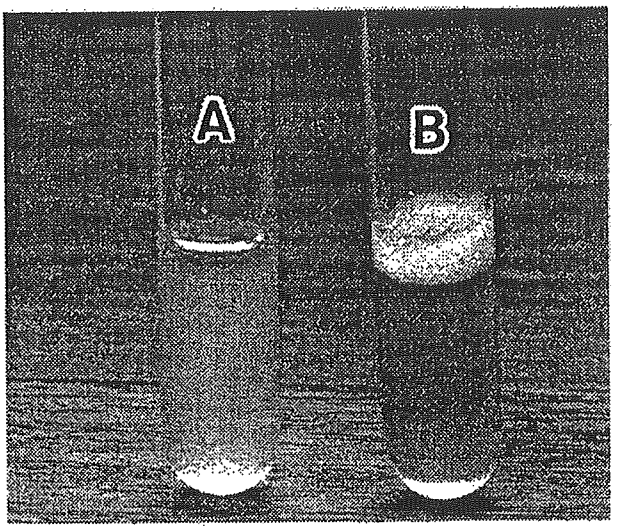

Figure 3. Homogenous bacterial suspension of *V. cholerae* O139 smooth strain in a static culture (A) and biofilm formation of rugose O139 under the same culture conditions (B).

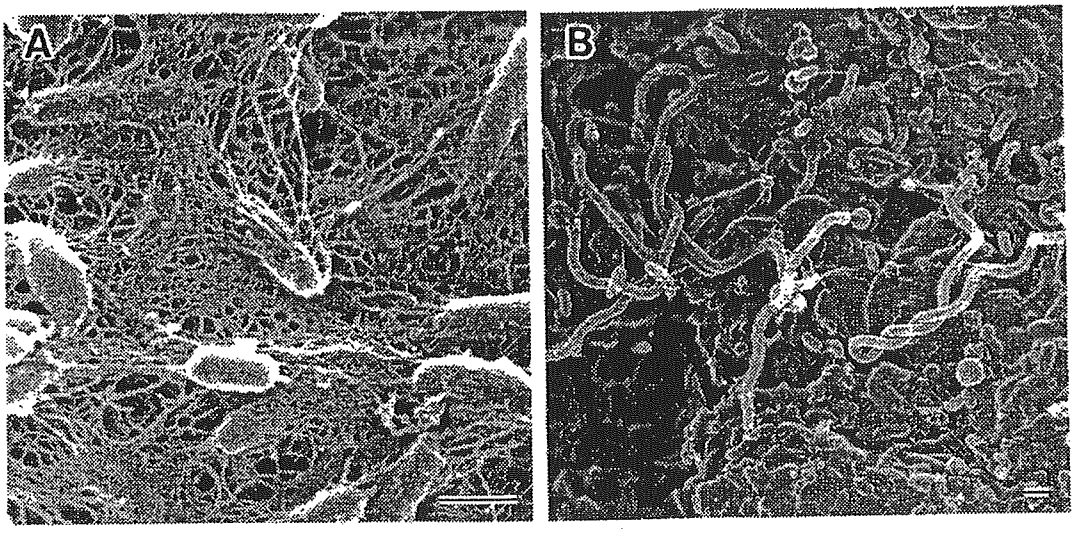

Figure 4. Scanning electron micrographs of biofilm formed by *V. cholerae* rugose strain. (A) Most of the surface has been colonized by rod cells, and finger-like projections of extracellular polymeric material are present. (B) The presence of twisting filamentous or rounded cells on biofillm. Bars, 1 μm.

rounded and contained less internally staining material and probably lost integrity. These cells were probably dead after only 2 days incubation (Fig. 5B). Bacteria in biofilm maintained the normal ultrastructure after 12 days incubation without addition of new nutrient (Fig. 5C). In a murine infection model, it was shown that uropathogenic *E. coli* (UPEC) is able to replicate intracellularly, forming highly organized biofilm-like community of coccoid

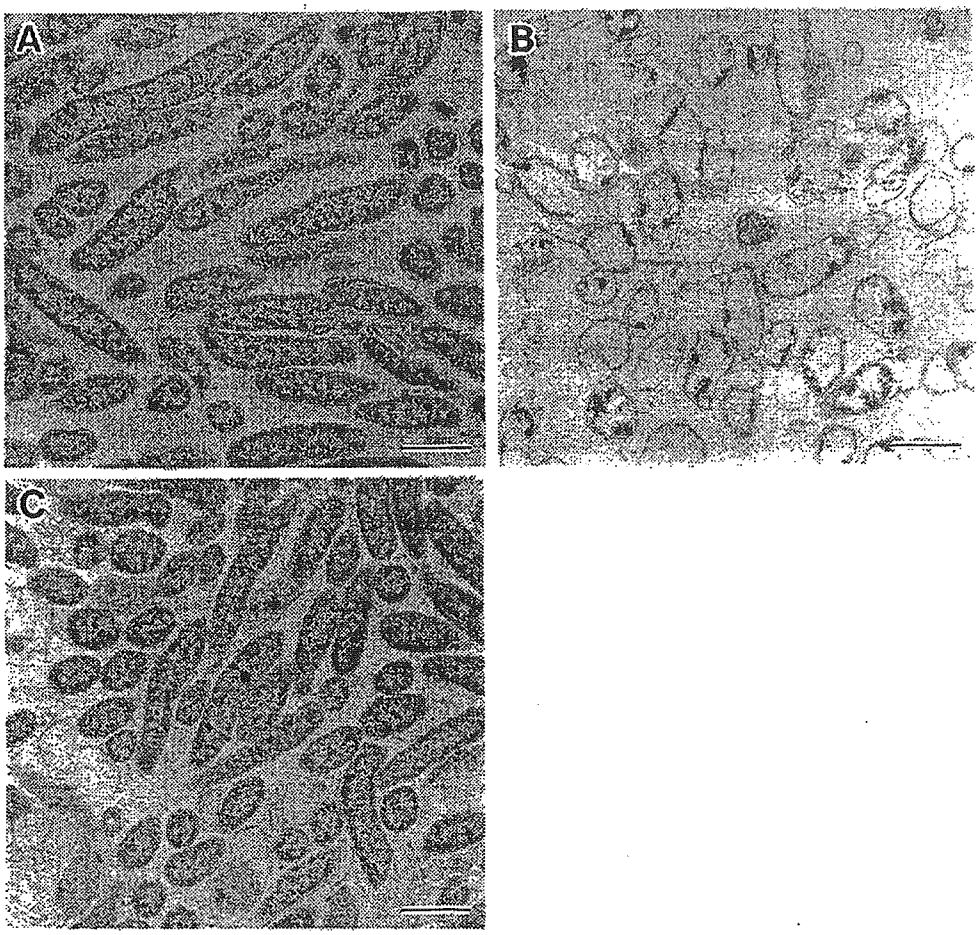

Figure 5. Thin-sectioning electron micrographs of *V. cholerae* cells. Cells in 2 days old biofilm, rod-shaped, with a uniform distribution of electron-dense ribosomal and nucleic acid materials throughout the cytoplasm (A). Two days old planktonic cells, mostly rounded, containing less internally staining materials (B). Cells in 12 days old biofilm showing the normal ultrastructure (C). Bars, 1 μm.

bacteria that ultimately filled most of the cytoplasm, creating a bulge on the bladder surface giving the appearance of a pod (24, 56). Bacteria within the superficial umbrella cells can escape into the bladder lumen in a process termed fluxing. Often, these fluxing bacteria are filamentous (56). Recruited polymorphonuclear leukocytes (PMNs) fail to gain access to the intracellular bacteria and to pagocytose the filamentous bacteria. Intracellular growth and filamentation provided an advantage to the bacteria in evading infiltrating PMNs (26). Biofilm formation and biofilm related morphological change such as filamentation appear to confer the advantage to survive the stress conditions in both host and external environments to organisms.

Molecular genetic analysis of *V. cholerae* biofilm formation demonstrated that EPS production requires a chromosomal locus, *vps* (*Vibrio* polysaccharide synthesis), that contains sequences homologous to carbohydrate biosynthesis